arXiv:0810.4923v2 [astro-ph] 8 Jan 2009

# IMPROVED STANDARDIZATION OF TYPE II-P SUPERNOVAE: APPLICATION TO AN EXPANDED SAMPLE

Dovi Poznanski[1], Nathaniel Butler[1,2], Alexei V. Filippenko[1], Mohan Ganeshalingam[1], Weidong Li[1], Joshua S. Bloom[1,3], Ryan Chornock[1], Ryan J. Foley[1,4,5], Peter E. Nugent[6], Jeffrey M. Silverman[1], S. Bradley Cenko[1], Elinor L. Gates[7], Douglas C. Leonard[8], Adam A. Miller[1], Maryam Modjaz[1], Frank J. D. Serduke[1], Nathan Smith[1], Brandon J. Swift[9], and Diane S. Wong[1]

*ApJ accepted December 2, 2008*

## ABSTRACT

In the epoch of precise and accurate cosmology, cross-confirmation using a variety of cosmographic methods is paramount to circumvent systematic uncertainties. Owing to progenitor histories and explosion physics differing from those of Type Ia SNe (SNe Ia), Type II-plateau supernovae (SNe II-P) are unlikely to be affected by evolution in the same way. Based on a new analysis of 17 SNe II-P, and on an improved methodology, we find that SNe II-P are good standardizable candles, almost comparable to SNe Ia. We derive a tight Hubble diagram with a dispersion of 10% in distance, using the simple correlation between luminosity and photospheric velocity introduced by Hamuy & Pinto (2002). We show that the descendent method of Nugent et al. (2006) can be further simplified and that the correction for dust extinction has low statistical impact. We find that our SN sample favors, on average, a very steep dust law with total to selective extinction $R_V < 2$. Such an extinction law has been recently inferred for many SNe Ia. Our results indicate that a distance measurement can be obtained with a single spectrum of a SN II-P during the plateau phase combined with sparse photometric measurements.

*Subject headings:* cosmology: observations — distance scale — dust, extinction — supernovae: general

## 1. INTRODUCTION

Compelling evidence for cosmic acceleration comes from distance measurements to Type Ia supernovae (SNe Ia; e.g., Astier et al. 2006; Wood-Vasey et al. 2007; Riess et al. 2007; Kowalski et al. 2008, see Filippenko 2005b for a review of earlier studies). Yet even with unlimited observational resources to improve statistical uncertainty, SN Ia cosmology ultimately faces systematic uncertainties stemming from an incomplete physical model of the phenomena. Indeed, since the physical conditions which give rise to the progenitors of the events are extremely difficult to discern, with no real consensus having been reached thus far, determining the nature of the evolution of SNe Ia at high redshift remains a crucial challenge for precise and accurate measurements of the fundamental cosmological parameters. While several mechanisms have been devised to measure, test, and constrain SN Ia systematics (e.g., Ellis et al. 2008; Foley et al. 2008), the possibility of source redshift evolution warrants a continued exploration of additional, complementary cosmographic methods.

A simple observation provides a compelling foundation for the use of Type II-plateau supernovae (SNe II-P) as standardizable candles: the progenitors of several SNe II-P have now been uncovered (e.g., Li et al. 2007; Smartt et al. 2008, and references therein), and all are found to be red supergiants with somewhat similar initial stellar masses (typically 8–16 $M_\odot$). Consequently, the environments and pre-SN evolution of such objects are reasonably tractable. Having undergone core collapse and envelope ejection, these red supergiants become SNe observationally defined by the presence of hydrogen in the spectra and a "plateau" phase in their light curves (e.g., Barbon et al. 1979, see Filippenko 1997 for a review). SNe II-P have been detected to redshift $z \approx 0.5$, and any evolutionary trends are likely to differ from those of SNe Ia.

As in the case of SNe Ia, the intrinsic inhomogeneity in SN II-P peak luminosity, and that produced by extrinsic factors such as dust, can be calibrated. There are two different approaches to determining distance: the theory-based method, and the empirical standardized-candle method. The theoretical approach branches into two: (1) the expanding photosphere method (EPM; Kirshner & Kwan 1975; Eastman et al. 1996), a historical descendent of the Baade-Wesselink method for variable stars (Baade 1926), and (2) the more modern "synthetic spectral atmosphere fitting" method (e.g., Baron et al. 2004; Dessart & Hillier 2006). Both techniques require the comparison of high signal-to-noise ratio (S/N) photometry and spectra of a given object to model atmospheres; for the second method,

Electronic address: dovi@berkeley.edu
[1] Department of Astronomy, University of California, Berkeley, CA 94720-3411.
[2] GLAST Fellow.
[3] Sloan Research Fellow.
[4] Harvard-Smithsonian Center for Astrophysics, 60 Garden Street, Cambridge, MA 02138.
[5] Clay Fellow.
[6] Lawrence Berkeley National Laboratory, 1 Cyclotron Road, Berkeley, CA 94720.
[7] Lick Observatory, PO Box 85, Mount Hamilton, CA 95140.
[8] Department of Astronomy, San Diego State University, Mail Code 1221, San Diego, CA 92182-1221.
[9] Steward Observatory, University of Arizona, Tucson, AZ 85721.

synthesized spectra are computed for each SN in detail. Distances based on improved versions of the theoretical modeling for a handful of well-observed SNe II-P have been shown to be precise to 10% (e.g., Leonard et al. 2003; Hamuy 2005; Baron et al. 2004; Dessart & Hillier 2006; Dessart et al. 2008), not greatly inferior to the best precision achievable with SNe Ia (7%; Astier et al. 2006). The requirement of high S/N observations, however, limits the efficacy of this approach for events at larger distances.

The standardized candle method first suggested by Hamuy & Pinto (2002; hereafter HP02) provides an independent empirical way to achieve distances to SNe II-P, and it is strongly anchored in simple physics. In more luminous SNe, the H-recombination front is maintained at higher velocities; the photosphere is farther out in radius. When a SN II-P is on the plateau phase of its light curve (which lasts for around 100 rest-frame days), there is a strong correlation between the velocity of the weak Fe II lines near $5000 \, \text{Å}$ – that trace the photospheric velocity – and the luminosity on the plateau. Extinction corrections are based on a variety of different methods. This empirical correlation was further studied by Hamuy (2005; hereafter H05); application to 24 SNe II-P in the Hubble flow yields a Hubble diagram in the $I$ band with a scatter of 15% in distance.

Nugent et al. (2006; hereafter N06) modified this technique by simultaneously combining both the extinction correction (using the rest-frame $V - I$ color on the plateau) and the Fe II velocity correction to arrive at a simple correlation between these parameters and luminosity. Given the smaller quantity of the data required, the N06 method, or a variant thereof, is probably the only framework that could be followed cost-effectively at high redshifts.

The number of SNe II-P for which distances have been derived, using any available method, is $\sim$20. The paucity of such objects, and the intractable biases that emerge from the way the sample was constructed, warrants an analysis of more SNe, and push for improved and better-tested correlations that will allow one to achieve the precision and control of systematics that could make these SNe competitive tools for precision cosmology.

In this work, we add 17 new objects to the current sample of low-$z$ SNe II-P, almost doubling the size, and reanalyze 3 previously published events. We discuss the full sample construction in §2. In §3 we present and modify the N06 fitting method. We discuss in §4 the sample culling, derive a new Hubble diagram, and find that the scatter is $\sim$10% in distance; we also consider the robustness and possible biases in the method, and compare distances derived for SNe that occurred in the same host galaxy, checking for internal consistency. Our conclusions are summarized in §5.

## 2. THE SUPERNOVA SAMPLE

### 2.1. *The Previously Existing Samples*

N06 compiled a list of 24 SNe II-P, 6 of which had not yet been published; one new event (SN 2004dh) was studied as part of the Caltech Core Collapse Project (CCCP; Gal-Yam et al. 2007) and is at low redshift, while the other 5 are at moderate redshifts, $0.1 < z < 0.3$, found in the course of the Supernova Legacy Survey (Astier et al. 2006). The other 18 SNe, previously collected by H05 and HP02, were found and observed between 1986 and 2000, with a variety of instruments. All of those SNe had $z < 0.06$, though the majority were at $z < 0.01$. For such nearby objects peculiar velocities of the host galaxies dominate the error budget, thus complicating the derivation of robust correlations and distances.

Since a "standard" Hubble diagram of distance modulus vs. redshift assumes that the sole contribution to the redshifts is cosmological, we apply corrections to the heliocentric redshifts in order to account for the peculiar velocities of nearby galaxies. Following previous authors, in the analysis below we correct the heliocentric redshifts derived from the SNe and their host galaxies to the local Hubble flow using the Tonry et al. (2000) prescription. We further assume a Hubble constant $H_0 = 70 \, \text{km} \, \text{s}^{-1} \text{Mpc}^{-1}$. Since we later fit for the absolute magnitude of the SNe, $H_0$ merely serves as a convenient scaling constant. For SN 1999em, we derive a redshift using the Hubble law and the Cepheid distance measured by Leonard et al. (2003), $11.7 \pm 1 \, \text{Mpc}$. We re-reduced the images of SN 2004dh and report here new photometry for that event. Finally, following H05, we remove SN 2000cb from the sample, since it is now believed to be a SN 1987A-like event rather than a classic SN II-P. Hereafter we will refer to these 23 SNe as the "HPN sample" (for Hamuy, Pinto, and Nugent).

### 2.2. *The KAIT Sample: Nearly Doubling the Low-Redshift Census*

The 0.76-m Katzman Automatic Imaging Telescope (KAIT) is mostly known as the SN discovery engine of the Lick Observatory SN Search (LOSS; Filippenko et al. 2001; Filippenko 2005a), but a substantial fraction of its time is dedicated to follow-up broadband photometry of nearby SNe. As part of this program, dozens of SNe II have been monitored in the past ten years. We select the SNe II-P from the KAIT sample, since other core-collapse SN subtypes are not necessarily expected to obey the same correlations. However, the SN II-P subclass is not well defined. While historically SNe were classified by their light-curve shapes, and SNe with a distinctive plateau were dubbed SNe II-P (e.g., Barbon et al. 1979; Doggett & Branch 1985), it is unclear how constant a plateau must be, how long that phase must last, and in which photometric bands it appears. In fact, those SNe which show hydrogen in their spectra but photometrically decline linearly (in magnitudes) were called SNe II-L, but not a single one of the best-studied objects (e.g., SN 1979C) is considered a "normal" prototype (e.g, Poznanski et al. 2002, and references therein; Poznanski et al. 2009, in prep.).

With the modern emphasis shifting to spectroscopic follow-up observations, the classification becomes, dishearteningly, even muddier. It is often assumed by SN observers that only SNe II-P exhibit hydrogen lines having P-Cygni profiles (e.g., Schlegel 1996), but this claim has not been explored systematically. Lately, several core-collapse SNe with extreme luminosities have been discovered (e.g., Ofek et al. 2007; Smith et al. 2007, 2008; Quimby et al. 2007; Miller et al. 2008; Gezari et al. 2008), stretching the classification scheme beyond its current limits.

TABLE 1
KAIT Sample

| IAU Name | Heliocentric $cz$ (km s$^{-1}$) | Flow $cz$[a] (km s$^{-1}$) | $t_{\rm expl}$[b] | $v_{\rm Fe\,II}$[c] (km s$^{-1}$) | $m_I$[d] (mag) | $V - I$[d] (mag) | Discovery Reference |
|---|---|---|---|---|---|---|---|
| SN1999bg[e] | 1275 | 1214(187) | 1259(5) | 4657(439) | 15.31(0.02) | 0.74(0.04) | Li (1999a) |
| SN1999em | 717 | 819( 70)[f] | 1476(4) | 3382(171) | 13.23(0.03) | 0.58(0.03) | Li (1999b) |
| SN1999gi | 592 | 643(187) | 1520(4) | 3697(200) | 14.00(0.02) | 0.86(0.03) | Nakano & Kushida (1999) |
| SN2000bs | 8387 | 8387(187) | 1650(6) | 4115(276) | 17.67(0.09) | 0.51(0.10) | Papenkova & Li (2000) |
| SN2000dc[e] | 3117 | 3113(187) | 1762(4) | 4545(232) | 16.05(0.06) | 0.97(0.06) | Yu & Li (2000) |
| SN2000dj | 4629 | 4625(187) | 1789(7) | 4784(250) | 17.00(0.09) | 0.59(0.11) | Aazami & Li (2000) |
| SN 2001x | 1480 | 1329(187) | 1964(5) | 3800(203) | 14.74(0.02) | 0.57(0.03) | Li et al. (2001a) |
| SN2001bq | 2623 | 2238(187) | 2034(6) | 4023(238) | 15.55(0.03) | 0.51(0.08) | Nakano et al. (2001) |
| SN2001cm | 3412 | 3413(187) | 2064(0) | 4065(189) | 16.30(0.02) | 0.68(0.03) | Jiang & Qiu (2001) |
| SN2001cy[e] | 4478 | 4473(187) | 2086(6) | 3987(218) | 16.13(0.04) | 0.63(0.05) | Ganeshalingam et al. (2001) |
| SN2001do[e] | 3124 | 3121(187) | 2134(2) | 3927(311) | 15.75(0.03) | 0.97(0.05) | Modjaz & Li (2001) |
| SN2002gd[e] | 2674 | 2418(187) | 2551(2) | 2774(315) | 16.78(0.03) | 0.74(0.05) | Klotz et al. (2002) |
| SN2002hh | 48 | 297(187) | 2576(2) | 3692(435) | 13.68(0.05) | 2.67(0.05) | Li (2002) |
| SN2003hl | 2472 | 2105(187) | 2868(4) | 3561(293) | 15.60(0.02) | 0.98(0.04) | Li (2003) |
| SN2003iq | 2472 | 2105(187) | 2921(1) | 4043(179) | 15.27(0.03) | 0.66(0.03) | Llapasset (2003) |
| SN2004du[e] | 5025 | 5020(187) | 3223(4) | 4855(302) | 16.60(0.04) | 0.53(0.07) | Singer & Li (2004) |
| SN2004et | 48 | 297(187) | 3272(0) | 3980(194) | 11.39(0.01) | 0.52(0.01) | Zwitter et al. (2004) |
| SN2005ay | 809 | 816(187) | 3453(4) | 3432(224) | 14.67(0.02) | 0.63(0.06) | Rich (2005) |
| SN2005cs | 463 | 505(187) | 3550(1)[g] | 2102(211) | 13.98(0.02) | 0.69(0.03) | Kloehr et al. (2005) |

[a] Corrected velocity of recession using the local Hubble-flow model of Tonry et al. (2000), unless otherwise noted.
[b] Explosion date, assumed to be the midpoint epoch (given as Julian Day $-$ 2,450,000) between the time of discovery and the last nondetection (the uncertainty being half this value), unless otherwise noted.
[c] Fit velocity of the Fe II line at day 50, on the plateau.
[d] Measured at day 50, on the plateau.
[e] Not used in the final sample, see §4.1.
[f] From the Cepheid distance of Leonard et al. (2003) and the Hubble law.
[g] From Pastorello et al. (2006).

For the purpose of this work, we define the SN II-P subclass as follows: (a) prominent hydrogen features in the spectra, (b) no narrow emission lines indicative of interaction with the circumburst medium, and (c) a prominent "plateau" phase in the $I$-band light curve.

The light-curve shape criterion is intentionally defined here rather loosely, so as not to preselect the best objects (beyond unavoidable observational biases) and is revisited in detail in §4.1. Several dozen SNe in the KAIT sample pass these criteria, but for 19 of them we have the data necessary for empirical calibration and distance measurement; they constitute the main sample analyzed here (Table 1). The SNe II-P that were not selected for this work were usually missing early-phase photometry to constrain the explosion date, or lacked spectroscopic coverage during the plateau, as required for measuring velocities. Two of our 19 chosen SNe (SN 1999em and SN 1999gi) are already present in the HPN sample; they are very well-studied objects (e.g., Hamuy et al. 2001; Leonard et al. 2002a,b; Dessart & Hillier 2006). We have used them to ascertain that there are no systematic offsets between our magnitude and velocity measurements and those of previous authors. Thus, our sample consists of 17 new SNe II-P.

The optical CCD images of the SNe were reduced as follows. Flat-fielding and bias subtraction were performed automatically at the telescope using calibration frames appropriate for the science images. Galaxy subtraction and differential photometry were done using the KAIT pipeline (Ganeshalingam et al. 2009, in prep.). Galaxy template images were obtained with KAIT at least a few months after the SN had faded beyond detection. To ensure high-quality subtractions, templates were acquired on photometric nights with seeing $\leq 3.0''$. Two independent routines were used to perform galaxy subtraction. The first method is based on the ISIS package (Alard & Lupton 1998) as modified by Brian P. Schmidt for the High-$z$ Supernova Search Team (Schmidt et al. 1998). The second method is based on the IRAF[10] task PSFMATCH (Phillips & Davis 1995). We performed differential point-spread function (PSF) fitting photometry to the results of both subtraction methods using the DAOPHOT package in IRAF to measure the SN flux relative to local standards in the field. The results of the two subtraction methods were averaged.

Calibrations were obtained on photometric nights using both KAIT and the 1 m Nickel telescope at Lick Observatory. Landolt (1992) standards were observed at a variety of airmasses on each night to derive a photometric solution that we then applied to local standards for each of the SN fields. Instrumental magnitudes were transformed to standard Johnson-Cousins magnitudes using color terms derived from the photometric solution of many Landolt standard-star calibrations (see Modjaz et al. 2001 and Li et al. 2001b for more details). The uncertainty in our subtraction and photometry pipeline is estimated by injecting artificial stars with the same magnitude and PSF as the SN into the original KAIT images and recovering them. The final uncertainty is taken to be the scatter in recovering 20 artificial stars added in quadrature with the calibration error. We correct the magnitudes for Galactic extinction using the maps of Schlegel et al. (1998).

---

[10] IRAF: the Image Reduction and Analysis Facility is distributed by the National Optical Astronomy Observatories, which is operated by the Association of Universities for Research in Astronomy, Inc. (AURA) under cooperative agreement with the National Science Foundation (NSF).
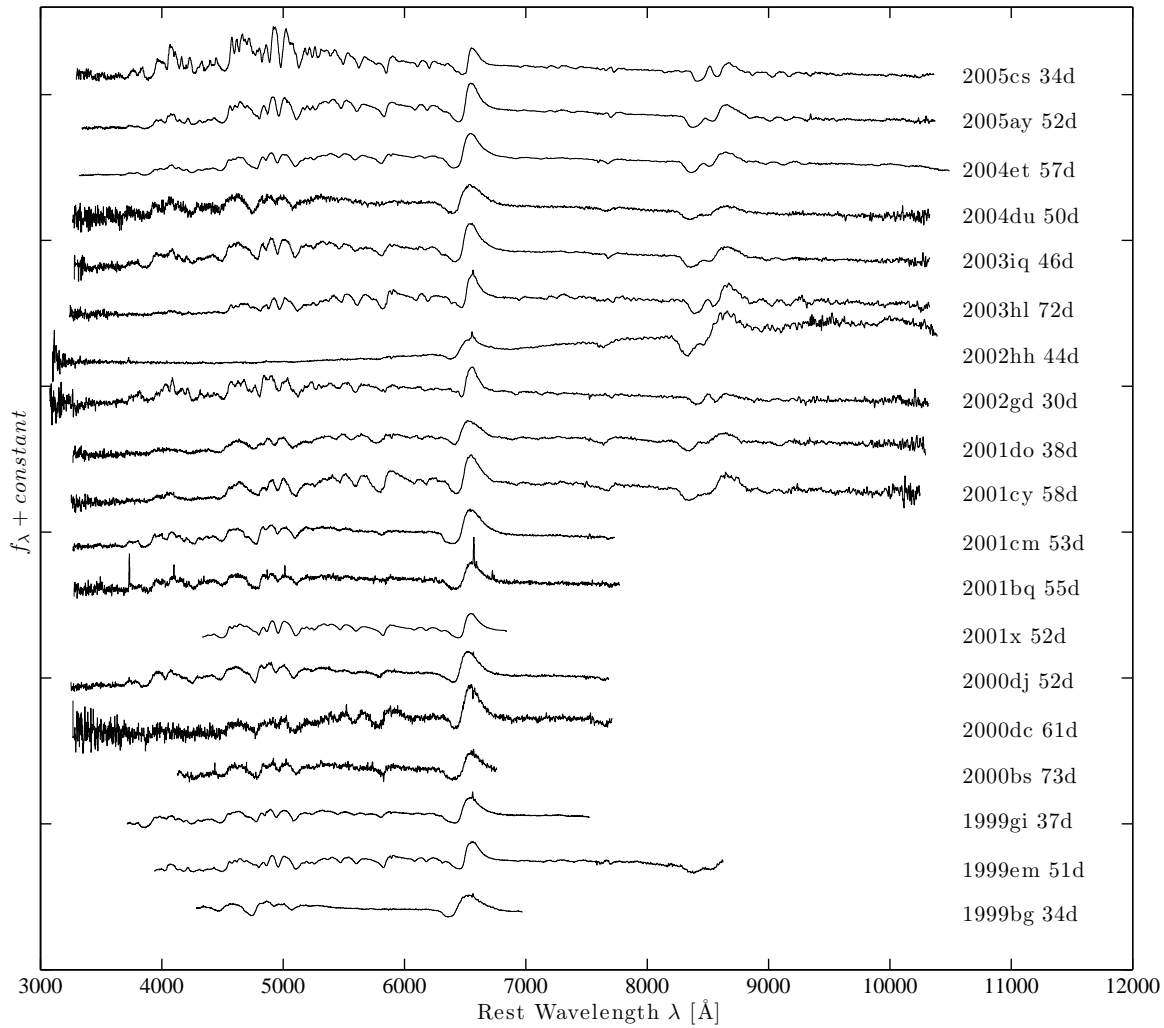
Fig. 1.— A representative spectrum (the closest to day 50) for each of the 19 SNe in our sample. The analysis herein makes use of about 75 spectra of these 19 events.

We obtained optical spectra with the Kast double spectrograph (Miller & Stone 1993) mounted on the Lick Observatory 3 m Shane telescope, the Low Resolution Imaging Spectrometer (LRIS; Oke et al. 1995) mounted on the 10 m Keck I telescope, and the Deep Imaging Multi-Object Spectrograph (DEIMOS; Faber et al. 2003) on the 10 m Keck II telescope. The position angle of the slit was generally aligned along the parallactic angle to reduce differential light losses (Filippenko 1982).

All spectra were reduced using standard techniques (e.g., Foley et al. 2003). Routine CCD processing and spectrum extraction for the Kast and LRIS data were completed with IRAF. These data were extracted with the optimal algorithm of Horne (1986). CCD processing of the DEIMOS spectra was performed with a modified version of the DEEP pipeline (e.g., Weiner et al. 2005). This produced rectified, sky-subtracted two-dimensional spectra from which one-dimensional spectra were then extracted optimally (Horne 1986). The wavelength scale was derived from low-order polynomial fits to calibration-lamp spectra. Small wavelength shifts were then applied to the data after cross-correlating a template night-sky spectrum to the sky spectrum extracted near the SN position on the slit. Using custom routines, we fit spectrophotometric standard-star spectra to the data in order to flux calibrate the spectra and to remove telluric lines (Wade & Horne 1988; Matheson et al. 2000). Information regarding both our photometric and spectroscopic data (such as observing conditions, instrument, data reducer, etc.) was obtained from our SN database (SNDB). The SNDB uses the popular open-source software stack known as LAMP: the Linux operating system, the Apache webserver, the MySQL relational database management system, and the PHP server-side scripting language (Silverman et al. 2009, in prep.). Figure 1 shows one spectrum of each of the 19 chosen SNe.

Figure 2 presents the $BVRI$ light curves of our 19 SNe, and shows the epochs at which spectra were obtained. In total, there are about 1500 photometric points and 75 spectra used in this study. A thorough analysis of these data is beyond the scope of this paper, and will be discussed by Poznanski et al. (2009, in prep.). However, we note the great diversity of plateau shapes, a subject to which we return in §4.1.

From the light curves we determine, using linear interpolation where necessary, the apparent magnitude in the $I$ band and the $V-I$ color at 50 d past explosion. We set the explosion date conservatively as the midpoint between the last nondetection of the SN and its discovery date (and the uncertainty as half this interval), except for SN 2005cs where we
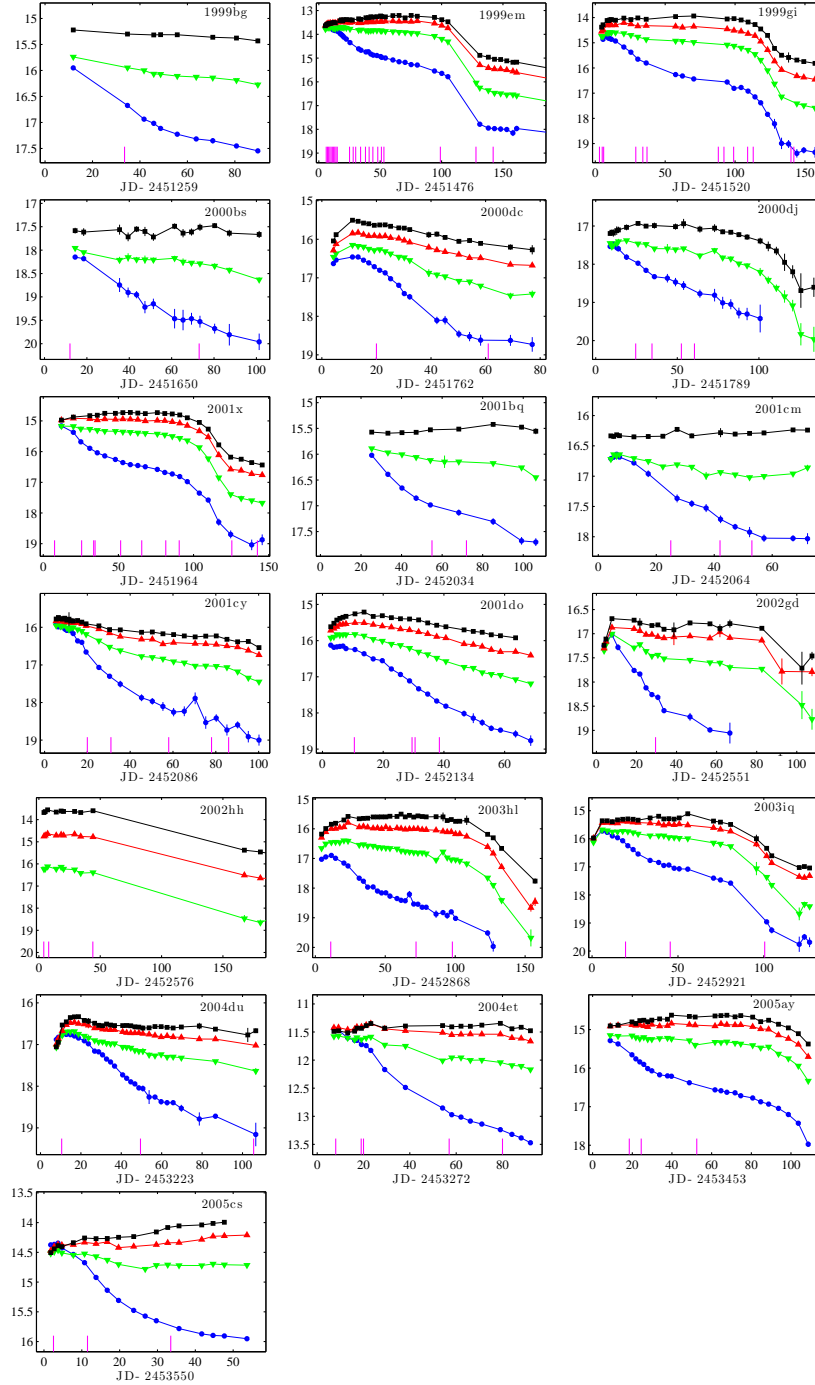
FIG. 2.— Light curves of the 19 SNe II-P from KAIT: $B$ (blue dots), $V$ (green upside-down triangles), $R$ (red triangles), and $I$ (black squares). Vertical line segments at the bottom of each panel mark the times for which we have spectra. Note the abundance of spectra, and the diversity in the SN light-curve shapes.

use the constraint determined by Pastorello et al. (2006). For many objects better constraints on the explosion date could be set by using additional techniques (e.g., fitting templates to the photometry and/or spectroscopy); however, the explosion-date uncertainties have little impact on our results, since neither the color nor the magnitude (or Fe II velocities, see below) vary significantly during the plateau phase. We have well-sampled light curves, and as can be seen in Figure 1, we have spectra near day 50 for most of our SNe.

Since the KAIT filter system differs somewhat from the Bessell curves used by N06, we also $S$-correct (Stritzinger et al. 2002) the photometry to the standard Bessell $BVRI$ curves taken from the database of Moro & Munari (2000). We do the correction by warping a standard day 50 template spectrum to the KAIT photometry, and measuring synthetic magnitudes using the Bessell filter response. This has no noticeable influence on our results, since the corrections are all smaller than 2% in the measured values.

From the spectra we measure the apparent Fe II velocity, defined here as the minimum of the Fe II line with respect to 5169 Å. Unfortunately, there is no "industry standard" framework to determine the velocities of such broad, often
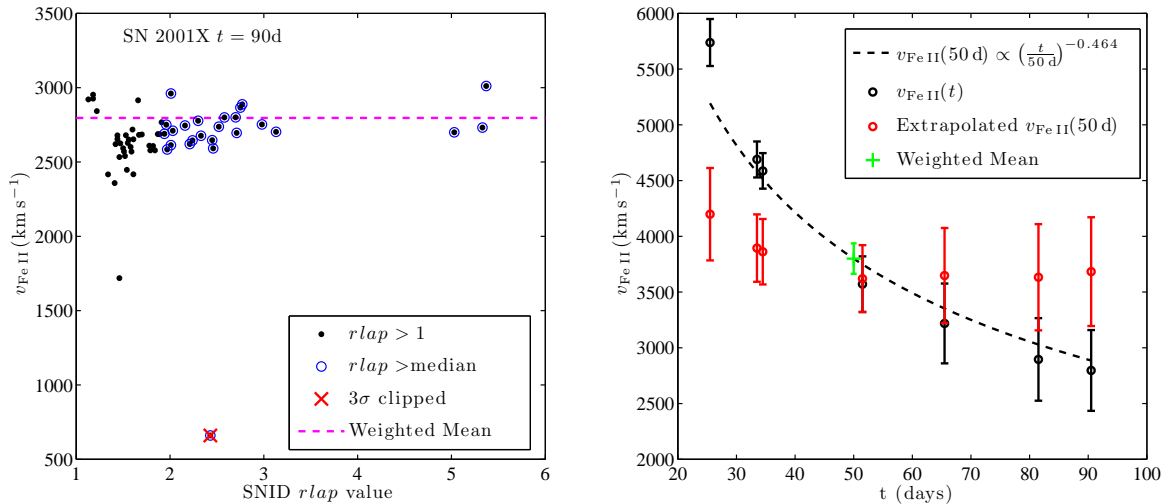
FIG. 3.— *Left:* Example application of our SNID-based Fe II velocity measurement to a typical spectrum. A day 90 spectrum of SN 2001X is cross-correlated with a set of templates using SNID, and a velocity is derived from each template (black dots). The best-fitting templates are selected based on SNID *rlap* values (blue circles), and sigma clipped to reject outliers (red crosses). A weighted mean is calculated from the selected velocities. *Right:* For a given object (SN 2001X in this example), each velocity (black circles) is propagated to day 50 (red circles) using Equation (2) of N06 (dashed line; our Equation (1)). A weighted mean supplies the final Fe II velocity for that SN, and its uncertainty. An additional uncertainty of $150 \, \mathrm{km \, s^{-1}}$ is added in quadrature to every SN, to account for peculiar motion.

noisy, and sometimes asymmetric lines; the different approaches we tried reveal systematic differences in the derived values and hence different calibration parameters. In an effort to develop a method that is simple, robust, and readily available to the community, we decided to use the supernova identification code (SNID; Blondin & Tonry 2007), originally designed for the automatic spectral classification of SNe. It uses the Tonry & Davis (1979) cross-correlation algorithm, and is flexible enough to be used for our purpose.

Figure 3 shows an example application of our method. We use the high-quality SN II-P templates distributed with SNID, for which the Fe II absorption-minimum wavelengths can be measured in a straightforward way (e.g., by fitting a Gaussian to the line). We then cross-correlate every spectrum with the templates (using only the relevant wavelength range, 4500–5500 Å), choose only those templates that produce a good fit (those with SNID *rlap* values greater than the median for the group), and calculate a sigma-clipped ($3\sigma$) weighted mean (left panel of Fig. 3). We convert the wavelength offsets to velocity using the relativistic Doppler formula. Each velocity (and its uncertainty) is then propagated to day 50 on the plateau using Equation (2) of N06,

$$v_{\mathrm{Fe \, II}}(50 \, \mathrm{d}) = v_{\mathrm{Fe \, II}}(t)(t/50 \, \mathrm{d})^{0.464 \pm 0.017}. \qquad (1)$$

Since most SNe have more than one available spectrum, we calculate for each SN the weighted mean of all derived Fe II velocities (right panel of Fig. 3). We add to the velocity uncertainty of every SN a value of $\sigma_{\mathrm{pec}} = 150 \, \mathrm{km \, s^{-1}}$, in quadrature, to account for unknown peculiar velocities within the hosts (Sofue & Rubin 2001). We have also confirmed that Equation (1) is consistent with our spectra, and we find no substantial residual from the N06 result, within its uncertainty.

As for the HPN sample, the apparent heliocentric redshifts of the SN hosts are derived from NED[11] and corrected for local flows using the model of Tonry et al. (2000). The properties of SNe in our sample, as measured above, are included in Table 1.

## 2.3. *Sample Comparison*

To understand whether HPN and KAIT sample a similar population, we compare the relevant observables in both samples. Figure 4 shows a comparison of the distribution of uncorrected absolute *I*-band magnitudes (top panel), $V - I$ colors (middle), and Fe II velocities (bottom), all at day 50 on the plateau, as measured above. These are the quantities used for standardization and distance measurement. Surprisingly, the luminosity distributions appear consistent with each other, while the KAIT sample features redder colors indicating a higher average extinction, and lower velocities that point to lower luminosities.

Using Kolmogorov-Smirnov (KS) statistics, we find that the luminosity distributions match reasonably well ($P_{\mathrm{K-S}}$ values of 0.66), whereas the colors and velocities are less consistent ($P_{\mathrm{K-S}}$ values of 0.13 and 0.06, respectively). Those results remain similar if one considers only $z < 0.1$ SNe. However, the high-velocity objects in the HPN sample all have substantial uncertainties that are not taken into account by KS statistics. For example, most of the highest-velocity SNe in the HPN samples have velocity uncertainties of $2000 \, \mathrm{km \, s^{-1}}$. Nevertheless, differences in sample properties should be expected, due to the era in which they were compiled. KAIT is expected to be sensitive to fainter SNe, either intrinsically (hence with lower average velocities) or due to dust obscuration (hence with red colors). One should

---

[11] The NASA/IPAC Extragalactic Database is operated by the Jet Propulsion Laboratory, California Institute of Technology, under contract with the National Aeronautics and Space Administration.
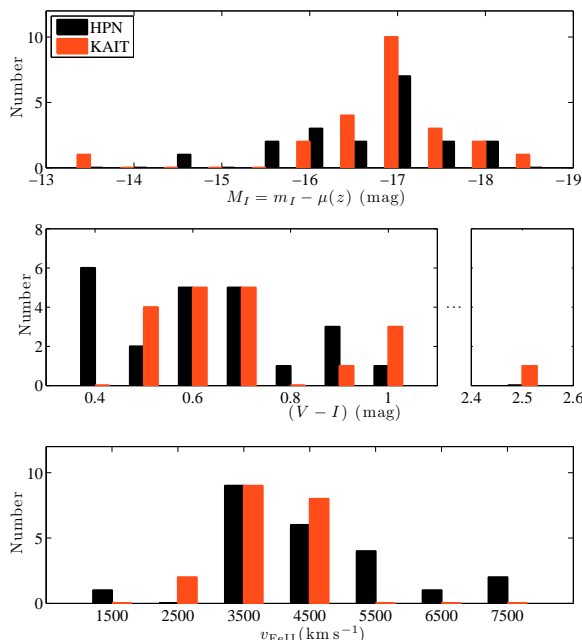
FIG. 4.— Comparison of the HPN and KAIT samples, showing observables relevant for distance measurements. Uncalibrated absolute magnitude (i.e., without applying dust or Fe II velocity correction; top), $V-I$ (middle), and Fe II velocity (bottom). KS statistics indicate that the samples can be assumed to be drawn from the same underlying distribution at high significance for the absolute magnitude, but quite low significance for the color and Fe II velocities.

note that while the KAIT sample may be less biased than the HPN sample, the luminosity function is still skewed significantly toward bright objects, due to follow-up criteria, as the median absolute magnitude is $0.5-1$ mag brighter than the observed distribution of all KAIT SNe II-P (i.e., including those SNe that were not scheduled for follow-up observations; Li et al. 2009, in prep.). While the importance of this bias should be explored with future more balanced samples, we note that at high redshift the same selection naturally occurs. The difference between the samples in terms of the observed properties has a visible effect on the Hubble diagram we construct, as discussed in §4.2.

With an absolute magnitude distribution spanning more than 5 mag and a diverse set of light-curve shapes (Fig. 2), the standardizability of SNe II-P would appear to be a significant challenge. However, as we demonstrate below, the resultant Hubble diagram remains tight, and the velocity vs. luminosity correlation persists, despite the larger and less homogeneous sample.

Using the 23 SNe in the HPN sample, and the 19 in the KAIT sample, we construct our list of 40 SNe, after merging the two shared SNe, SN 1999em and SN 1999gi. For these two SNe we use the KAIT measurements, due to the somewhat smaller uncertainties (but consistent values) we obtain for the observables. Table 2 lists the full sample used in the subsequent analysis.

## 3. FITTING METHOD

N06 assume a correlation between luminosity and Fe II velocity that is only modified by a Cardelli et al. (1989) extinction law, with $R_V = 3.1$. However, there is no *a priori* reason to assume that all of the SNe in the sample are subject to the same extinction law, with the average curvature found in the Milky Way. For that reason we modify the color-dependent term in Equation (1) of N06 to be a free parameter. This term, which has a value of 1.36 in N06[12], we refer to as $R_I$. Given the color excess $E(V-I) \equiv (V-I) - (V-I)_0$, $R_I$ defines the amount of extinction in the $I$ band, such that $A_I = R_I E(V-I)$. The value of $R_I$ can be directly derived from the Cardelli et al. (1989) extinction curve as a function of $R_V$. We therefore obtain a slightly modified Equation (1) of N06:

$$M_I = M_{I_0} - \alpha \log_{10}(v_{\text{Fe II}}/5000) + R_I \left[ (V-I) - (V-I)_0 \right]. \tag{2}$$

In addition, we use "Hubble-constant free" absolute magnitudes and luminosity distances $\mathcal{M}_{I_0} \equiv M_{I_0} - 5 \log_{10}(H_0) + 25$ and $\mathcal{D}_L \equiv H_0 D_L$ (Goobar & Perlmutter 1995; Sullivan et al. 2006), since we use no anchor of "absolute" distance, and measure only the shape of the Hubble diagram (relative distances). We thus find

$$\mathcal{M}_{I_0} - \alpha \log_{10}(v_{\text{Fe II}}/5000) + R_I \left[ (V-I) - 0.53 \right] - m_I = -5 \log_{10}(\mathcal{D}_L(z|\Omega_m, \Omega_\Lambda)), \tag{3}$$

where we use for the ridge-line color the value from N06, $(V-I)_0 = 0.53$ mag. As mentioned by N06, the precise value for this color is degenerate with $\mathcal{M}_{I_0}$, and does not influence our other results. As seen in the middle panel of fig. 4, perhaps due to the ubiquity of dust around SNe II-P, or as a consequence of an intrinsic dispersion, it is difficult to find a precise value for the unreddened color of those SNe.

Since all of the terms in Equation (3) have errors, including significant redshift uncertainties for the nearby SNe, we maximize the marginal likelihood $\mathcal{L}$ by minimizing the multivariate cost function

---

[12] Note the sign misprint in N06 for that term.

TABLE 2
FINAL SAMPLE

| Name[a] | $cz/z$[b] (km s$^{-1}$) | $v_{\mathrm{Fe\,II}}$[c] (km s$^{-1}$) | $m_I$[c] (mag) | $V - I$[c] (mag) | Best-fit $\mu$ (mag) | Source |
|---|---|---|---|---|---|---|
| SN2002hh | 297(187) | 3692( 435) | 13.68(0.05) | 2.67(0.05) | 28.89(0.23) | KAIT |
| SN2004et | 297(187) | 3980( 194) | 11.39(0.01) | 0.52(0.01) | 28.36(0.09) | KAIT |
| SN2005cs | 505(187) | 2102( 211) | 13.98(0.02) | 0.69(0.03) | 29.61(0.21) | KAIT |
| SN1999gi | 643(187) | 3697( 200) | 14.00(0.02) | 0.86(0.03) | 30.57(0.13) | KAIT |
| SN1999br | 757(187) | 1545( 300) | 16.67(0.05) | 0.84(0.07) | 31.60(0.43) | N06 |
| SN2005ay | 816(187) | 3432( 224) | 14.67(0.02) | 0.63(0.06) | 31.27(0.13) | KAIT |
| SN1999em | 819( 70)[d] | 3382( 171) | 13.23(0.03) | 0.58(0.03) | 29.84(0.11) | KAIT |
| SN1991G | 1029(187) | 3347( 500) | 15.01(0.09) | 0.45(0.11) | 31.70(0.36) | N06 |
| SN1992ba | 1064(187) | 3523( 300) | 14.65(0.05) | 0.59(0.07) | 31.33(0.18) | N06 |
| SN1989L | 1189(187) | 3529( 300) | 14.47(0.05) | 0.88(0.07) | 30.94(0.19) | N06 |
| SN1986I | 1190(187) | 3623( 300) | 13.98(0.09) | 0.45(0.22) | 30.82(0.29) | N06 |
| SN1990E | 1273(187) | 5324( 300) | 14.51(0.20) | 1.31(0.28) | 31.44(0.37) | N06 |
| SN2001x | 1329(187) | 3800( 203) | 14.74(0.02) | 0.57(0.03) | 31.59(0.11) | KAIT |
| SN1990K | 1623(187) | 6142(2000) | 13.87(0.05) | 0.58(0.21) | 31.62(0.75) | N06 |
| SN2003hl | 2105(187) | 3561( 293) | 15.60(0.02) | 0.98(0.04) | 32.01(0.14) | KAIT |
| SN2003iq | 2105(187) | 4043( 179) | 15.27(0.03) | 0.66(0.03) | 32.16(0.10) | KAIT |
| SN2001bq | 2238(187) | 4023( 238) | 15.55(0.03) | 0.51(0.08) | 32.55(0.13) | KAIT |
| SN1999ca | 2772(187) | 5353(2000) | 15.56(0.05) | 0.73(0.07) | 32.93(0.89) | N06 |
| SN2001cm | 0.011(0.001) | 4065( 189) | 16.30(0.02) | 0.68(0.03) | 33.18(0.10) | KAIT |
| SN1991al | 0.013(0.001) | 7330(2000) | 16.06(0.05) | 0.39(0.07) | 34.28(0.54) | N06 |
| SN2000dj | 0.015(0.001) | 4784( 250) | 17.00(0.09) | 0.59(0.11) | 34.26(0.18) | KAIT |
| SN1992af | 0.016(0.001) | 5322(2000) | 16.46(0.20) | 0.43(0.28) | 34.05(0.87) | N06 |
| SN2004dh | 0.017(0.001) | 4990( 300) | 17.60(0.15)[e] | 0.70(0.21)[e] | 34.86(0.30) | N06 |
| SN1999cr | 0.019(0.001) | 4389( 300) | 17.44(0.05) | 0.56(0.07) | 34.56(0.18) | N06 |
| SN1999eg | 0.019(0.001) | 4012( 300) | 17.72(0.05) | 0.55(0.07) | 34.68(0.16) | N06 |
| SN1993A | 0.027(0.001) | 4290( 300) | 18.56(0.05) | 0.51(0.07) | 35.68(0.17) | N06 |
| SN2000bs | 0.028(0.001) | 4115( 276) | 17.67(0.17) | 0.51(0.20) | 34.71(0.31) | KAIT |
| SN1993S | 0.029(0.001) | 4569( 300) | 18.22(0.05) | 0.69(0.07) | 35.32(0.14) | N06 |
| SN1992am | 0.042(0.001) | 7868( 300) | 17.90(0.05) | 0.38(0.07) | 36.27(0.11) | N06 |
| SN04D4fu | 0.119(0.001) | 3861( 150) | 21.99(0.04) | 0.59(0.05) | 38.85(0.11) | N06 |
| SN03D4cw | 0.138(0.001) | 3067( 660) | 22.33(0.09) | 0.90(0.10) | 38.52(0.47) | N06 |
| SN04D1pj | 0.139(0.001) | 4981( 214) | 21.99(0.04) | 0.66(0.06) | 39.28(0.11) | N06 |
| SN04D1ln | 0.185(0.001) | 3593( 159) | 22.79(0.05) | 0.70(0.07) | 39.43(0.12) | N06 |
| SN03D3ce | 0.257(0.001) | 5762( 522) | 23.45(0.50) | 0.39(0.50) | 41.22(0.79) | N06 |
| | | | | | | |
| Culled SNe | | | | | | |
| | | | | | | |
| SN1999bg | 1214(187) | 4657( 439) | 15.31(0.02) | 0.74(0.04) | 32.41(0.18) | KAIT |
| SN2002gd | 2418(187) | 2774( 315) | 16.78(0.03) | 0.74(0.05) | 32.90(0.21) | KAIT |
| SN2000dc | 0.010(0.001) | 4545( 232) | 16.05(0.06) | 0.97(0.06) | 32.93(0.14) | KAIT |
| SN2001do | 0.010(0.001) | 3927( 311) | 15.75(0.03) | 0.97(0.05) | 32.35(0.15) | KAIT |
| SN2001cy | 0.015(0.001) | 3987( 218) | 16.13(0.04) | 0.63(0.05) | 33.01(0.12) | KAIT |
| SN2004du | 0.017(0.001) | 4855( 302) | 16.60(0.04) | 0.53(0.07) | 33.94(0.13) | KAIT |

[a] Sorted by increasing redshift.
[b] From local Hubble-flow model of Tonry et al. (2000) (unless otherwise noted). For $cz > 3000$ km s$^{-1}$ the redshift is given.
[c] At day 50, on the plateau.
[d] From the Cepheid distance of Leonard et al. (2003) and the Hubble law.
[e] Note that these numbers differ from those in N06, following our re-reduction of the data.

$$-2\log(\mathcal{L}) = \sum \{ \frac{[\mathcal{M}_{I_0} - \alpha \log_{10}(v_{\mathrm{Fe\,II}}/5000) + R_I\left[(V-I) - 0.53\right] - m_I + 5\log_{10}(\mathcal{D}_L(z))]^2}{\alpha\sigma^2_{\log_{10}(v_{\mathrm{Fe\,II}}/5000)} + R_I\sigma^2_{(V-I)} + \sigma^2_{m_I} + \sigma^2_{5\log_{10}(\mathcal{D}_L(z))} + \sigma^2_{\mathrm{sys}}}$$
$$+ \log(\alpha\sigma^2_{\log_{10}(v_{\mathrm{Fe\,II}}/5000)} + R_I\sigma^2_{(V-I)} + \sigma^2_{m_I} + \sigma^2_{5\log_{10}(\mathcal{D}_L(z))} + \sigma^2_{\mathrm{sys}}) \}, \tag{4}$$

where the summation is over the SNe in the sample (e.g., Kelly 2007). The second, logarithmic term — which comes from the normalization of the likelihood function — helps mitigate the tendency of the first term to overfit the data by preferring large values of $\alpha$, $R_I$, and $\sigma_{\mathrm{sys}}$. We note, however, that this term does not significantly change the resulting best-fit parameters. We include in the denominator (and the logarithmic term) of Equation (4) a systematic uncertainty $\sigma_{\mathrm{sys}}$ in order to include (and measure) the intrinsic scatter in the correlation (i.e., the contribution to the dispersion not accounted for by the measurement errors).

The parameters to be fit are therefore $\mathcal{M}_{I_0}$ (although for simplicity we will keep citing values for $M_{I_0}$, assuming $H_0 = 70\,\mathrm{km\,s^{-1}\,Mpc^{-1}}$), $\alpha$, $R_I$ (that we translate to $R_V$), $\sigma_{\mathrm{sys}}$, and the cosmological parameters. For the present low-$z$ data, since we do not have any leverage on the cosmological parameters, we assume a standard cosmology ($\Omega_m = 0.3$, $\Omega_\Lambda = 0.7$), and only fit for $\sigma_{\mathrm{sys}}$ and the correlation coefficients.
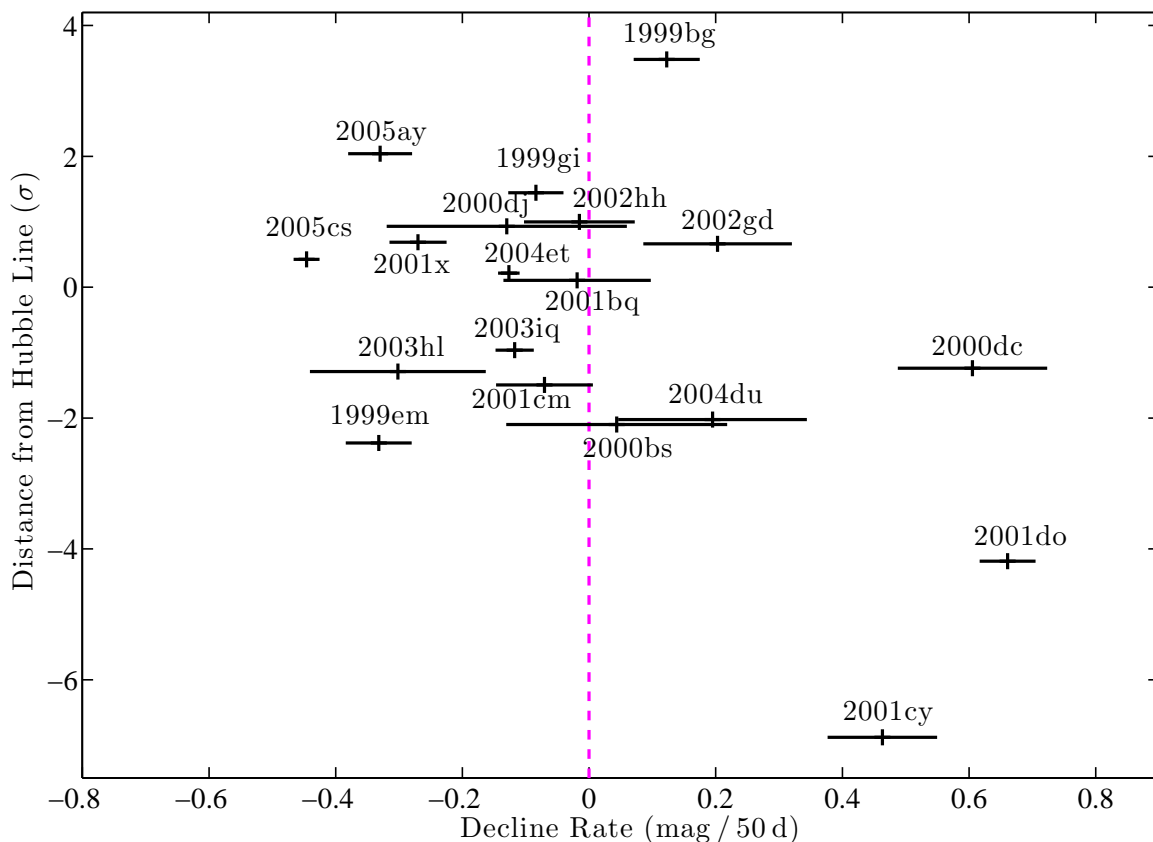
FIG. 5.— Offset from the Hubble law fit to the full sample before culling, as a function of the $I$-band decline rate. As can be clearly seen, SN 2001cy and SN 2001do are amongst the strongest decliners and are our most significant outliers, followed by SN 1999bg which declines as well. The magenta dashed line marks our cutoff, where we select only SNe that have decline rates smaller than (or consistent to $1\sigma$ with) zero.

## 4. RESULTS

Using the complete sample of 40 SNe, we find that the best-fit values after marginalization are $\alpha = 4.6 \pm 0.7$, $R_V = 1.5 \pm 0.5$ ($R_I = 0.7^{+0.3}_{-0.4}$), $M_{I_0} = -17.43 \pm 0.10$ mag, and $\sigma_{\rm sys} = 0.38$ mag. The systematic scatter is equivalent to an 18% uncertainty in distance, largely dominating the error budget, being more than twice the median measurement uncertainty. However, about a third of that scatter is due to two SNe in the KAIT sample, SN 2001cy and SN 2001do, and to some lesser extent SN 1999bg. Those SNe are offset from the best-fit solution by $6.7\sigma$, $4.1\sigma$, and $3.6\sigma$, respectively. An analysis excluding those objects gives a tight correlation with $\sigma_{\rm sys} = 0.22$ mag, which corresponds to 10% in distance.

### 4.1. Sample Culling for Cosmology

A possible glimpse at the source of the discrepancy lies in the photometric behavior of the outlying SNe. This is portrayed in Figure 5, where we show, for the KAIT SNe, the distance from the Hubble law (as derived from the complete sample) in $\sigma$ units, as a function of the decline rate in the $I$ band. We define here the decline rate as the slope of a linear fit to the $I$-band light curve starting 10 d after explosion (after the rise time), and ending at day 50, in units of mag $(50 \text{ d})^{-1}$. The errors are estimated using a Monte-Carlo simulation propagating the uncertainties in the photometry and in the explosion dates.

Figure 5 shows that SN 2001cy and SN 2001do have substantial decline rates, about 0.5 mag $(50 \text{ d})^{-1}$, while most objects barely decline, or even have rising light curves. The decline vs. offset correlation is not strong; consequently, adding a decline parameter to the fitting only marginally improves the scatter to $\sigma_{\rm sys} = 0.33$ mag. However, we can now define quantitatively a selective subsample of SNe II-P for the purpose of distance measurement in this paper, and reject objects in a controlled manner. For the purpose of this work, we will keep objects that have decline rates smaller than (or consistent to $1\sigma$ with) zero.[13]

As can be seen in Figure 5, this criterion rejects all three outliers (SNe 2001cy, 2001do, and 1999bg) by design, but also SNe 2000dc, 2002gd, and 2004du that are relatively well fit. This choice leaves 34 SNe in the combined sample that we analyze in the following sections. We emphasize that a similar cut has been applied by N06 prior to the

---

[13] Note that we are defining the specific subsample of SNe II-P in this way only for the purpose of having a clear and clean set for cosmological purposes. We do *not* mean to imply that every SN II having a decline rate larger than zero is necessarily a SN II-L or some other "not-II-P" SN. The real distinction between SNe II-P, SNe II-L, and other potential SN II subtypes will be considered in more detail by Poznanski et al. (2009, in prep.).
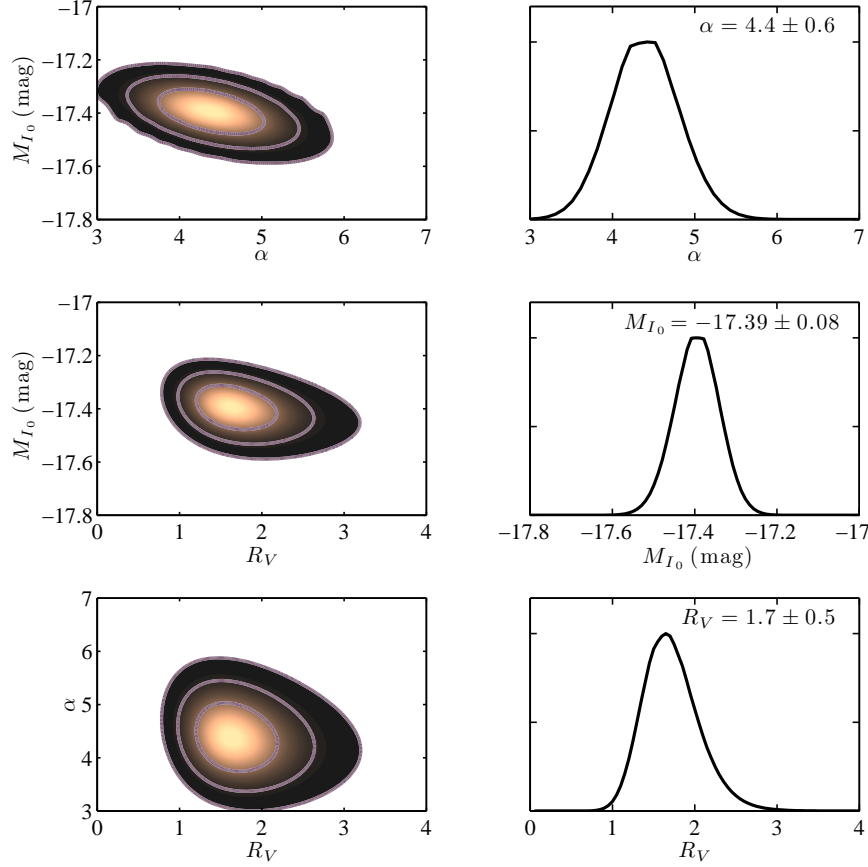
FIG. 6.— Best-fit parameter $(\alpha, M_{I_0}, R_V)$ $1\sigma$, $2\sigma$, and $3\sigma$ contours at left; marginalized posterior probabilities at right, for the culled sample of 34 SNe.

costly follow-up observations of the moderate-$z$ SNe in their sample (P. Nugent, 2008, private comm.), and has most probably been applied to the HP02 sample as well. The precise criteria have not been detailed previously, and could significantly bias the best-fit parameters and dispersion. Our choice, while somewhat arbitrary, does not affect our results below, and any choice that rejects the two major outliers will effectively be equivalent.

### 4.2. *Best-Fit Parameters and Hubble Diagram*

Using the culled sample of 34 SNe, we find that the best-fit values after marginalization are $\alpha = 4.4 \pm 0.6$, $R_V = 1.7 \pm 0.5$ $(R_I = 0.8 \pm 0.3)$, $M_{I_0} = -17.39 \pm 0.08$ mag, and $\sigma_{\mathrm{sys}} = 0.22$ mag (10% in distance), consistent with the values for the complete sample. The likelihood contours and the marginalized posteriors are plotted in Figure 6. As can be seen, the coefficients are weakly covariant.

The value of the best-fit average $R_V$, while small, is consistent with results for many SNe Ia, which tend to suffer an extinction that is very selective (Elias-Rosa et al. 2006; Krisciunas et al. 2007; Elias-Rosa et al. 2008; Nobili & Goobar 2008; Wang et al. 2008). As shown by Wang (2005) and Goobar (2008), this result could be explained with a fairly simple model where "normal," yet circumstellar, dust causes heavily color-dependent scattering. While this model is discussed in the context of SNe Ia, core-collapse SNe are expected (and observed) to be enshrouded by more circumstellar dust, which could explain these low $R_V$ values. We note that a small $R_V$ is still the best fit if one removes the highly extinguished SN 2002hh from the analysis.

Using Equation (3) we build the Hubble diagram in Figure 7. The scatter around the standard cosmology trend is quite small, and is accounted for by the systematic and measurement uncertainties. The systematic scatter can be contained in a reasonable velocity dispersion of $\sigma_{v_{\mathrm{Fe\,II}}} = 135\,\mathrm{km\,s^{-1}}$. This is equivalent to, or better than, the results obtained by previous authors, and is encouraging considering the size of the sample and its initial inhomogeneity.

### 4.3. *Robustness of the Correlation*

In order to test the robustness of the correlation, we explore the importance of the different ingredients in the fit. If one applies *no correction at all* (i.e., assume the SNe II-P are perfect standard candles), the correlation crumbles, and gives $\sigma_{\mathrm{sys}} \approx 0.9$ mag. The same occurs if one does not apply the velocity correction, but only the color correction. A simple test of the importance of that term is obtained by shuffling the velocity measurements among the objects, assigning to each SN a random value chosen from the sample distribution. The result, on average, is a very weak correlation, with $\sigma_{\mathrm{sys}} \approx 0.6$ mag, and unrealistic best values for the coefficients ($\alpha < 0$ and $R_V > 15$ in most cases; see Draine 2003 for a review on measured values and theoretical limits on $R_V$).
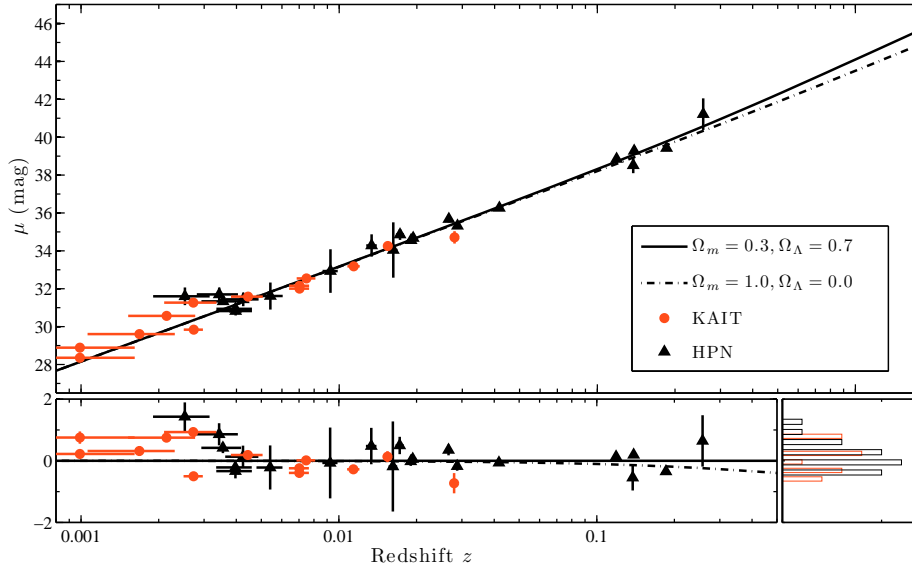
Fig. 7.— Hubble diagram (top), and residuals from standard concordance cosmology (bottom), for the HPN sample (black triangles) and the culled KAIT sample (orange filled circles). "Standard" (line) and Einstein-deSitter (dash-dot) cosmologies are added to guide the eye. The bottom-right panel shows the similarity in the distribution of residuals for both samples.

However, if we use solely the Fe II correction (which is numerically equivalent to setting $R_I = 0$ or $R_V = 0.78$), we get a scatter only slightly greater than for the best solution ($\sigma_{\rm sys} \approx 0.26$ mag), and mildly different values for $\alpha$ and $M_{I_0}$. This result indicates that for our sample of SNe, the dust correction is not strongly required by the data.

Since we *do* expect SN magnitudes to be affected by dust, there are a few possible explanations we consider. First, it could be that an intrinsic color-velocity correlation masks most of the contribution from dust. While theoretically one could expect the color (i.e., the temperature) to be correlated with the photospheric velocity at least to some extent, we find no indication in the sample for any such covariance, despite having at least a few SNe suffering negligible extinctions.

An alternative explanation is that the sample is heavily biased toward dust-free objects. While this is securely wrong for at least one object (SN 2002hh, which suffers ~5 mag of extinction in the $V$ band; Pozzo et al. 2006), it is probably wrong for many of the other SNe as well. H05 finds significant dust corrections for at least some of the SNe in his sample, and our sample should be less "hand-picked" as the objects included were discovered by modern-era CCD-equipped SN searches that can find more SNe II-P buried in their host galaxies.

However, neglecting SN 2002hh, most SNe in the sample are within $\sim 0.3$ mag of the sample's mean $V - I$ color. Additionally, for any reasonable dust law, the color term in Equation (3) is at least 3–5 times less significant than the velocity term, so that even substantial differences in color will contribute relatively little to the dispersion in distance moduli. Consequently, a sample that does not have many heavily extinguished objects can be fit about as well when assuming no extinction at all.

We have searched unsuccessfully for parameters that correlate with the residuals from the Hubble diagram and further reduce the necessary $\sigma_{\rm sys}$ value, other than the slope of the plateau in the light curve that we have used to cull our sample in §4.1. The $B$-band luminosity at day 50, for example, does not reduce the scatter by more than a few percent of its previous value. There are indications that rejection of red objects (those having $(V - I) - (V - I)_0 \gtrsim 0.2$ mag) may reduce the scatter, but our sample is still too small for us to make a robust statement regarding this.

We also determine the best-fit parameters for different subsamples of the data. The HPN and KAIT samples when analyzed separately give best-fit parameters consistent to within $1\sigma$ with those derived from the full set. When examining various cuts in redshift, we find that the lowest-redshift objects in the sample ($z \leq 0.004$) tend to pull the solutions to somewhat larger values of $\alpha$ (near 6 instead of 5), as previously noted by N06 and tentatively ascribed to a Malmquist bias. At $z \gtrsim 0.004$ there seems to be a systematic difference between the two samples, with the KAIT SNe being mostly underneath the Hubble-law line. The number of SNe in this range is too small for a conclusive analysis, but we estimate that this is a reflection of the differences between the samples noted in §2.3. KAIT finds intrinsically fainter and more extinguished SNe, for which the fit compensates by reducing their derived distances.

### 4.4. Shared-Host SNe

SN 2002hh and SN 2004et both occurred in the same host galaxy, NGC 6946, a neighbor of the Milky Way ($< 10$ Mpc away). While SN 2004et shows no apparent uniqueness (except perhaps some small photometric jitter in the plateau phase of the light curve), SN 2002hh is highly reddened by dust, with $A_V \approx 5$ mag and an infrared echo from a shell with $\sim 10$ M$_\odot$ (Barlow et al. 2005; Pozzo et al. 2006). Despite the extreme extinction, the distances of the two SNe, as derived using the best-fit parameters of §4.2, are consistent within about $2\sigma$ (see Table 2).

SN 2003hl and SN 2003iq exploded within weeks of each other, in the same host galaxy, NGC 772 (see Fig. 8, left panel). In fact, SN 2003iq was discovered by an amateur SN observer while following 2003hl (Llapasset 2003). With the exception of the first spectrum of SN 2003hl, our spectra were obtained by placing the slit on both objects
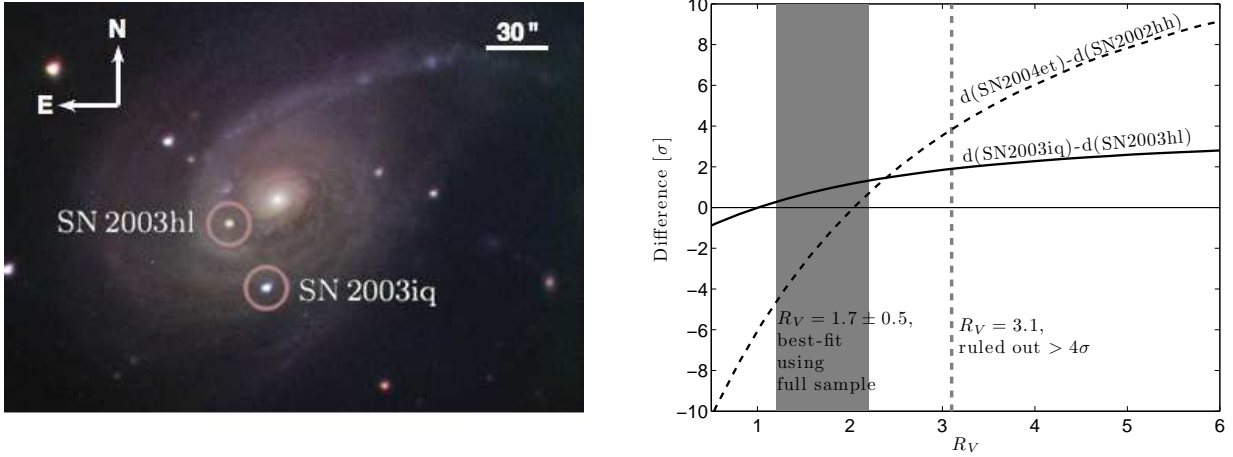
FIG. 8.— *Left:* Color composite image of NGC 772 showing SN 2003hl and SN 2003iq. It consists of KAIT *BVRI* images, and a deeper frame from Deep-Sky (Nugent et al. 2009, in prep.) not showing the SNe, but enhancing galaxy features. *Right:* Distance difference between SNe 2003hl and 2003iq (solid line) and between SNe 2002hh and 2004et (dashed line), in $\sigma$ units, as a function of the assumed $R_V$. A value of $R_V = 3.1$ (dashed grey line) is rejected at more than $4\sigma$. The gray area marks the $1\sigma$ interval preferred by the full sample. These two pairs of SNe, as well as the full sample, favor a low-$R_V$ dust model.

simultaneously. In this lower-extinction case (compared with SN 2002hh in NGC 6946), the agreement in distance is even better.

However, the distances to both pairs of SNe best agree only for the favored model with low $R_V$. (A similar value for SN 2002hh has been measured by Pozzo et al. 2006 using a full light-curve comparison to SN 1999em.) As seen in the right-hand panel of Figure 8, a value of $R_V = 3.1$ is rejected at a combined significance level higher than $4\sigma$. This result strongly supports the low $R_V$ value favored by the full sample.

### 4.5. *Error Budget: Prospects for Future Samples*

While the scatter we find in §4.2 is small, it is tightly coupled to our error estimates. The value $\sigma_{\rm sys} = 0.22$ mag is in effect the scatter unaccounted for by other error terms. As can be seen in Table 2, due to the quality of our data, our uncertainties are generally smaller than those of previous authors. If one argues that those uncertainties are underestimated (though we find that they are not), increasing them by some amount will result in an even smaller value of $\sigma_{\rm sys}$.

As a consequence of our precise measurements, systematic errors dominate our Hubble diagram. This allows us to constrain the intrinsic dispersion of the correlation to be roughly 10% in distance. However, one should note that there are observational limitations that would increase that uncertainty for any foreseeable sample. Even for data with exquisite photometry, and high S/N spectroscopy, there still remains an uncertainty in the peculiar velocity of the exploding star, on the order of $150\,{\rm km\,s^{-1}}$. This translates to about $0.05-0.08$ mag of uncertainty, i.e., $2-4\%$ in distance. A reasonable precision to expect for a SN with a single spectrum is about $300\,{\rm km\,s^{-1}}$, or $\sim 0.12$ mag.

In addition, any project that wishes to amass a suitable sample of SNe II-P will need to address the critical issue of sample definition discussed in §4.1. A simple strategy to overcome this would include high-cadence observations during a "detection phase," in order to have strong constraints on the explosion dates, followed by low-cadence monitoring of the candidates, in order to ascertain that they do not decline.

The weak dependence on $V-I$ color discussed in §4.3 has strong utility for extension to high-$z$ SNe, where selection against faint and reddened SNe is stronger, and dust could have less impact. A Hubble diagram based only on the $V$ band, without any color term, is equivalent to fixing $R_I = -1$ in Equation (3). Solving for the other parameters, we find a somewhat inferior scatter of $\sigma_{\rm sys} = 0.29$ mag. However, obtaining rest-frame $I$-band magnitudes for $z > 0.4$ SNe is observationally challenging, requiring near-infrared observations. The slightly poorer scatter in the $V$ band can be overcome by statistics. We do not expect significant scatter (or evolution) in those photometric bands due to metallicity. Figure 13 of Baron et al. (2003) shows that wildly different metallicities produce little variance in the intrinsic colors of SNe II-P at wavelengths longer than $\sim 5000$ Å. Future low-$z$ samples will also allow a better quantitative determination of the cutoff in decline rate that separates "good standardizable SNe II-P" from other SNe.

### 5. CONCLUSIONS

Using a sample that is larger and more diverse than those studied previously, we have shown that SNe II-P can be calibrated using simple correlations, yielding a tight Hubble diagram with a dispersion of $\sim 10\%$ in distance, not much worse than for SNe Ia, if one carefully constructs the sample of SNe. We have shown that the N06 standardization method, a derivative of the HP02 method, might be simplified even further because the correction for dust extinction, based on the current sample, has a low statistical impact on the scatter in the Hubble diagram. This implies that a distance measurement could, in principle, be obtained with a single spectrum of a SN during the plateau phase, combined with rest-frame $V$ or $I$-band photometry at a similar time. However, additional (lower S/N) photometry is required during the plateau phase, in order to reject non-II-P SNe.

If dust correction is applied, the best-fit solution prefers a very steep dust law, with $R_V < 2$, as recently indicated for SNe Ia. This may have significant implications for SN Ia cosmology, where systematic uncertainties currently dominate. It is further supported by two pairs of SNe that occurred in the same host galaxies, and whose distances agree only for low $R_V$ values.

The Hubble diagram in Figure 7 is dominated by nearby objects, where systemic velocities of the host galaxies govern the error bars. More exact values of the parameters, and more confidence in the method, will require the analysis of a sample of SNe in the Hubble flow. The most useful redshift range to calibrate the methods is $z \approx 0.05$–0.1, a distance that has been almost inaccessible until recently due to the requirement of a very large, and moderately deep, search. Pan-STARRS (Kaiser et al. 2002) and the Palomar Transient Factory (PTF; Rau et al. 2009, in prep.) will supply more SNe II-P than any follow-up program could realistically handle. If subsequent follow-up resources are allocated, those SNe will become the backbone of any cosmological use of SNe II-P, anchoring the correlation on more secure grounds.

## REFERENCES

Aazami, A. B., & Li, W. D. 2000, IAU Circ., 7490, 1

Alard, C., & Lupton, R. H. 1998, ApJ, 503, 325

Astier, P., et al. 2006, A&A, 447, 31

Baade, W. 1926, Astronomische Nachrichten, 228, 359

Barbon, R., Ciatti, F., & Rosino, L. 1979, A&A, 72, 287

Barlow, M. J., et al. 2005, ApJ, 627, L113

Baron, E., Nugent, P. E., Branch, D., & Hauschildt, P. H. 2004, ApJ, 616, L91

Baron, E., Nugent, P. E., Branch, D., Hauschildt, P. H., Turatto, M., & Cappellaro, E. 2003, ApJ, 586, 1199

Blondin, S., & Tonry, J. L. 2007, ApJ, 666, 1024

Cardelli, J. A., Clayton, G. C., & Mathis, J. S. 1989, ApJ, 345, 245

Dessart, L., & Hillier, D. J. 2006, A&A, 447, 691

Dessart, L., et al. 2008, ApJ, 675, 644

Doggett, J. B., & Branch, D. 1985, AJ, 90, 2303

Draine, B. T. 2003, ARA&A, 41, 241

Eastman, R. G., Schmidt, B. P., & Kirshner, R. 1996, ApJ, 466, 911

Elias-Rosa, N., et al. 2006, MNRAS, 369, 1880

—. 2008, MNRAS, 384, 107

Ellis, R. S., et al. 2008, ApJ, 674, 51

Faber, S. M., et al. 2003, in SPIE Proc., ed. M. Iye & A. F. M. Moorwood, Vol. 4841, 1657

Filippenko, A. V. 1982, PASP, 94, 715

—. 1997, ARA&A, 35, 309

Filippenko, A. V. 2005a, in The Fate of the Most Massive Stars, ed. R. Humphreys & K. Stanek (San Francisco: ASP, Conf. Ser. Vol. 332), 33

Filippenko, A. V. 2005b, in White Dwarfs: Cosmological and Galactic Probes, ed. E. M. Sion, S. Vennes, & H. L. Shipman (Dordrecht: Springer), 97

Filippenko, A. V., Li, W. D., Treffers, R. R., & Modjaz, M. 2001, in Small Telescope Astronomy on Global Scales, ed. B. Paczyński, W.-P. Chen, & C. Lemme (San Francisco: ASP, Conf. Ser. Vol. 246), 121

Foley, R. J., et al. 2008, ApJ, 684, 68

—. 2003, PASP, 115, 1220

Gal-Yam, A., Cenko, S. B., Fox, D. B., Leonard, D. C., Moon, D.-S., Sand, D. J., & Soderberg, A. M. 2007, in The Multicoloured Landscape of Compact Objects and Their Explosive Origins, ed. T. di Salvo, et al. (New York: AIP, Conf. 924), 297

Ganeshalingam, M., Modjaz, M., & Li, W. D. 2001, IAU Circ., 7655, 1

Gezari, S., et al. 2008, in press (arXiv:0808.2812)

Goobar, A. 2008, submitted (arXiv:0809.1094)

Goobar, A., & Perlmutter, S. 1995, ApJ, 450, 14

Hamuy, M. 2005, in Cosmic Explosions, ed. J.-M. Marcaide & K. W. Weiler (Berlin: Springer-Verlag, IAU Col. 192), 535

Hamuy, M., & Pinto, P. A. 2002, ApJ, 566, L63

Hamuy, M., et al. 2001, ApJ, 558, 615

Horne, K. 1986, PASP, 98, 609

Jiang, X. J., & Qiu, Y. L. 2001, IAU Circ., 7641, 3

Kaiser, N., et al. 2002, in SPIE Proc., ed. J. A. Tyson & S. Wolff, Vol. 4836, 154

Kelly, B. C. 2007, ApJ, 665, 1489

Kirshner, R. P., & Kwan, J. 1975, ApJ, 197, 415

Kloehr, W., Muendlein, R., Li, W., Yamaoka, H., & Itagaki, K. 2005, IAU Circ., 8553, 1

Klotz, A., Puckett, T., Langoussis, A., Wood-Vasey, W. M., Aldering, G., Nugent, P., & Stephens, R. 2002, IAU Circ., 7986, 1

Kowalski, M., et al. 2008, in press (arXiv:0804.4142)

Krisciunas, K., et al. 2007, AJ, 133, 58

Landolt, A. U. 1992, AJ, 104, 340

Leonard, D. C., Kanbur, S. M., Ngeow, C. C., & Tanvir, N. R. 2003, ApJ, 594, 247

Leonard, D. C., et al. 2002a, PASP, 114, 35

—. 2002b, AJ, 124, 2490

Li, W. 1999a, IAU Circ., 7135, 1

—. 1999b, IAU Circ., 7294, 1

—. 2002, IAU Circ., 8005, 1

—. 2003, IAU Circ., 8184, 1

Li, W., Fan, Y., Qiu, Y. L., Hu, J. Y., & Schwartz, M. 2001a, IAU Circ., 7591, 1

Li, W., et al. 2001b, PASP, 113, 1178

Li, W., Wang, X., Dyk, S. D. V., Cuillandre, J.-C., Foley, R. J., & Filippenko, A. V. 2007, ApJ, 661, 1013

Llapasset, J. 2003, IAU Circ., 8219, 2

Matheson, T., Filippenko, A. V., Ho, L. C., Barth, A. J., & Leonard, D. C. 2000, AJ, 120, 1499

Miller, A. A., et al. 2008, in press (arXiv:0808.2193)

Miller, J. S., & Stone, R. P. S. 1993, Lick Obs. Tech. Rep. 66, (Santa Cruz: Lick Obs.)

Modjaz, M., & Li, W. D. 2001, IAU Circ., 7682, 1

Modjaz, M., Li, W., Filippenko, A. V., King, J. Y., Leonard, D. C., Matheson, T., Treffers, R. R., & Riess, A. G. 2001, PASP, 113, 308

Moro, D., & Munari, U. 2000, A&AS, 147, 361

Nakano, S., Itagaki, K., Li, W. D., & Schwartz, M. 2001, IAU Circ., 7628, 2

Nakano, S., & Kushida, R. 1999, IAU Circ., 7329, 1

Nobili, S., & Goobar, A. 2008, A&A, 487, 19

Nugent, P., et al. 2006, ApJ, 645, 841

Ofek, E. O., et al. 2007, ApJ, 659, L13

Oke, J. B., et al. 1995, PASP, 107, 375

Papenkova, M., & Li, W. D. 2000, IAU Circ., 7406, 1

Pastorello, A., et al. 2006, MNRAS, 370, 1752

Phillips, A. C., & Davis, L. E. 1995, in Astronomical Data Analysis Software and Systems IV, ed. R. A. Shaw, H. E. Payne, & J. J. E. Hayes (San Francisco: ASP, Conf. Ser. Vol. 77), 297

Poznanski, D., Gal-Yam, A., Maoz, D., Filippenko, A. V., Leonard, D. C., & Matheson, T. 2002, PASP, 114, 833

Pozzo, M., et al. 2006, MNRAS, 368, 1169

Quimby, R. M., Aldering, G., Wheeler, J. C., Höflich, P., Akerlof, C. W., & Rykoff, E. S. 2007, ApJ, 668, L99

Rich, D. 2005, IAU Circ., 8500, 2

Riess, A. G., et al. 2007, ApJ, 659, 98

Schlegel, D. J., Finkbeiner, D. P., & Davis, M. 1998, ApJ, 500, 525

Schlegel, E. M. 1996, AJ, 111, 1660

Schmidt, B. P., et al. 1998, ApJ, 507, 46

Singer, D., & Li, W. 2004, IAU Circ., 8387, 1

Smartt, S. J., Eldridge, J. J., Crockett, R. M., & Maund, J. R. 2008, submitted (arXiv:0809.0403)

Smith, N., Chornock, R., Li, W., Ganeshalingam, M., Silverman, J. M., Foley, R. J., Filippenko, A. V., & Barth, A. J. 2008, ApJ, 686, 467

Smith, N., et al. 2007, ApJ, 666, 1116

Sofue, Y., & Rubin, V. 2001, ARA&A, 39, 137

Stritzinger, M., et al. 2002, AJ, 124, 2100

Sullivan, M., et al. 2006, AJ, 131, 960

Tonry, J. L., Blakeslee, J. P., Ajhar, E. A., & Dressler, A. 2000, ApJ, 530, 625

Tonry, J., & Davis, M. 1979, AJ, 84, 1511

Wade, R. A., & Horne, K. 1988, ApJ, 324, 411

Wang, L. 2005, ApJ, 635, L33

Wang, X., et al. 2008, ApJ, 675, 626

Weiner, B. J., et al. 2005, ApJ, 620, 595

Wood-Vasey, W. M., et al. 2007, ApJ, 666, 694

Yu, C., & Li, W. D. 2000, IAU Circ., 7476, 1

Zwitter, T., Munari, U., & Moretti, S. 2004, IAU Circ., 8413, 1